Operator-split computation of 3-D symmetric flow

A. Birman, N. Y. Har'El

Rafael Ballistic Center, Rafael, P.O.B. 2250, Haifa, Israel

J. Falcovitz, M. Ben-Artzi, U. Feldman

Institute of Mathematics, Hebrew University, Jerusalem 91904, Israel

Abstract: A finite-difference approximation for the 3-D fluid dynamical equations in Cartesian coordinates is obtained by operator-splitting based on the 1-D GRP scheme. The shock capturing capability of the 3-D scheme is examined using a spherically symmetric test problem, where a converging fluid is brought to rest by a single shock wave. The 3-D solution is found to be as accurate in the mean as the corresponding 1-D solution. However, the post-shock flow in the 3-D solution is found to be "noisier" than in the corresponding 1-D solution, indicating that the mechanism of operator-split shock capturing is not identical to that of the corresponding 1-D symmetric scheme.

Key words: Conservation laws scheme, operator splitting, shock capturing

1. Introduction

The Euler equations that govern the time-dependent flow of an inviscid fluid are routinely solved by conservation laws schemes, such as the GRP scheme. This scheme is specifically formulated in one space variable, and has been demonstrated to produce high-resolution solutions to shock wave phenomena (see references [Ben-Artzi and Falcovitz 1984] through [Falcovitz and Ben-Artzi 1995]). Finite-difference approximations to the three-dimensional Euler equations in Cartesian coordinates, are commonly obtained by applying a one-dimensional scheme in the framework of operator-splitting.

Operator splitting is based on analytic arguments proposed by Strang 1968, who showed that judicious sequencing of one-dimensional schemes having a second-order accuracy level, produces a second-order accurate integration of the corresponding multi-dimensional system. However, such arguments are valid only for smooth flows, and do not hold for flows containing discontinuities. We adopt here a test case of spherically-symmetric flow, for which a solution is obtainable from a one-dimensional (quasi) conservation laws scheme. This solution is then compared with the simulation obtained by treating the flow as three-dimensional, with the computation performed by an operator-split scheme.

Our primary observation in this study, is that the operator-split computation produces a solution that

agrees quite well with the corresponding symmetric solution.

We start the article with a description of the operator splitting scheme, and an outline of the symmetric test problem. This is followed by a presentation and discussion of the computation results, ending with some concluding remarks.

2. Operator splitting

The compressible flow of an inviscid fluid in space and and time (x, y, z, t) is governed by the equations:

$$\partial_t U + \partial_x F(U) + \partial_y G(U) + \partial_z H(U) = 0 \qquad (1)$$

$$U = \begin{bmatrix} \rho \\ \rho u \\ \rho v \\ \rho w \\ \rho E \end{bmatrix}, \ F(U) = \begin{bmatrix} \rho u \\ \rho u^2 + p \\ \rho uv \\ \rho uw \\ u(\rho E + p) \end{bmatrix},$$

$$G(U) = \begin{bmatrix} \rho v \\ \rho vu \\ \rho v^2 + p \\ \rho vw \\ v(\rho E + p) \end{bmatrix},$$

$$H(U) = \begin{bmatrix} \rho w \\ \rho wu \\ \rho wv \\ \rho w^2 + p \\ w(\rho E + p) \end{bmatrix},$$

$$e = E - (u^2 + v^2 + w^2)/2, \qquad (2)$$

$$p = (\gamma - 1)\rho e, \qquad \gamma = \text{constant} > 1. \qquad (3)$$

In (1) $\rho, p, e, E, (u, v, w)$ are, respectively, the density, pressure, specific energy, specific total energy and velocity components. A perfect gas equation-of-state is specifically assumed.

A second-order accurate finite-difference approximation to the system (1), based on the operator-splitting method suggested by Strang 1968, is constructed by first "splitting" (1) into the following set of three one-dimensional conservation laws:

$$\begin{aligned} \partial_t U + \partial_x F(U) &= 0, \\ \partial_t U + \partial_y G(U) &= 0, \qquad (4) \\ \partial_t U + \partial_z H(U) &= 0. \end{aligned}$$

Briefly stated, the integration of U over a small time Δt according to (1), is approximated by a sequence of three "consecutive" integration operations according to each of the 1-D conservation laws in (4), again over the same Δt.

Let $S_A(\Delta t)$, $S_B(\Delta t)$, $S_C(\Delta t)$, denote one-dimensional second-order accurate finite-difference approximation operators to the three conservation laws (4), respectively. We then claim that the five-operator sequence

$$S_A(\tfrac{1}{2}\Delta t)S_B(\tfrac{1}{2}\Delta t)S_C(\Delta t)S_B(\tfrac{1}{2}\Delta t)S_A(\tfrac{1}{2}\Delta t) \quad (5)$$

is a second-order accurate finite-difference approximation to the 3-D system (1). This is clearly an extension to the the three-operator sequence suggested by Strang 1968, namely $S_B(\tfrac{1}{2}\Delta t)S_C(\Delta t)S_B(\tfrac{1}{2}\Delta t)$, which, as shown by Strang, constitutes a second-order accurate finite-difference approximation to the respective sub-system of conservation laws in (y, z, t).

A further reduction of the split scheme (5) is obtained by considering the N-fold repetition of the sequence (5), occurring in the case of integration to time $T = N\Delta t$, where $N >> 1$. It is reasoned that consecutive half-step operator pairs can be lumped to full-step single operators, while retaining the second-order accuracy level. The reduced sequence thus becomes,

$$S_A(\Delta t)S_B(\tfrac{1}{2}\Delta t)S_C(\Delta t)S_B(\tfrac{1}{2}\Delta t). \quad (6)$$

Our 3-D split integration is performed according to the sequence (6), using as the finite-difference operator the second-order accurate GRP scheme.

In order to estimate the effects of split sequencing on simulation results, we also employed an "unsplit" integration scheme. By unsplit finite-difference integration we mean that the divergence terms per cubic cell are obtained by simultaneously summing up the fluxes on all six faces of the cube. This modification of an operator-split code requires intermediate storage of all flux components in three-dimensional arrays.

3. Converging spherical flow

Our test case is the spherically converging flow of a perfect gas, having the uniform initial conditions $[p_o, \rho_o, u_o] = [p_o, 1, -1]$, which for $p_o = 0$ reduces to Noh's problem (Noh 1987). The resulting flow is self-similar (i.e., dependent solely on the similarity variable $\xi = r/t$), where the inward-flowing fluid is compressed isentropically and "fed" into a spherical shock wave which brings the fluid to rest at elevated pressure and density. This shock wave propagates radially out at a constant speed. The equations governing the self-similar isentropic flow reduce to a set of two coupled ordinary differential equations for the velocity and speed of sound (u, c), as given by Taylor 1946. The boundary conditions for these equations are $u = u_o$ and $c = c_o$ at infinity, and the Rankine-Hugoniot shock relations at the shock front, with $u_1 = 0$ imposed on the post-shock velocity.

The Runge-Kutta (fourth-order) method was used to integrate this pair of ODE's to any desired level of accuracy. We subsequently refer to this solution as the "exact" solution. As shown in Fig. 1, the resulting self-similar solution is quite sensitive to the initial pressure p_o. Note that the higher the initial pressure, the higher the shock speed and the lower the jump across the shock. For our test problem we assume from now on the initial conditions $[p_o, \rho_o, u_o] = [0.006, 1, -1]$, and $\gamma = 5/3$, for which the post-shock state is $[p_1, \rho_1, u_1] = [18.577, 51.697, 0]$, and the shock speed is $u_s = 0.36428$.
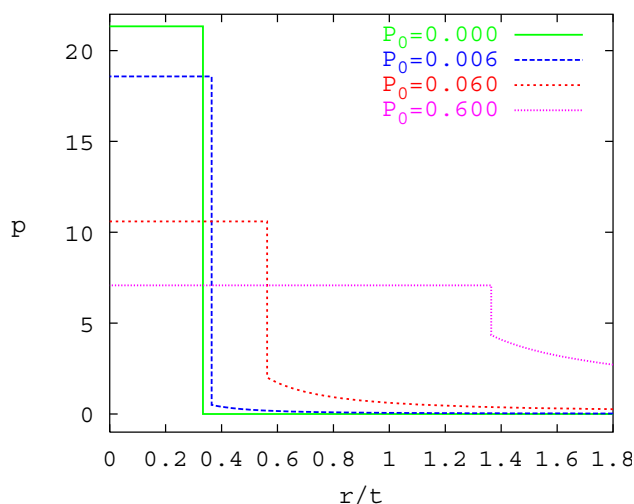

Figure 1. Pressure in self-similar flow for various p_o

4. Results and discussion

4.1. One-dimensional computation

The spherically symmetric flow is readily simulated in one space variable by the quasi conservation laws scheme GRP (see Ben-Artzi and Birman 1990, where the original Noh's problem was computed). The computation domain $0 < r < 100$ is divided into a grid of 100 equal cells, and the constant time step, which conforms to the CFL stability condition, is $\Delta t = 0.25$. The boundary conditions are: at the origin $u(0, t) = 0$, and at the outer boundary $p(100, t)$, $\rho(100, t)$, $u(100, t)$ are set equal to the corresponding exact solution (obtained by integrating the ODE as previously described). The computation is performed to the final time $t = 144$, where the shock front is at about $r_s = 52.5$. The results are shown in Fig. 2.
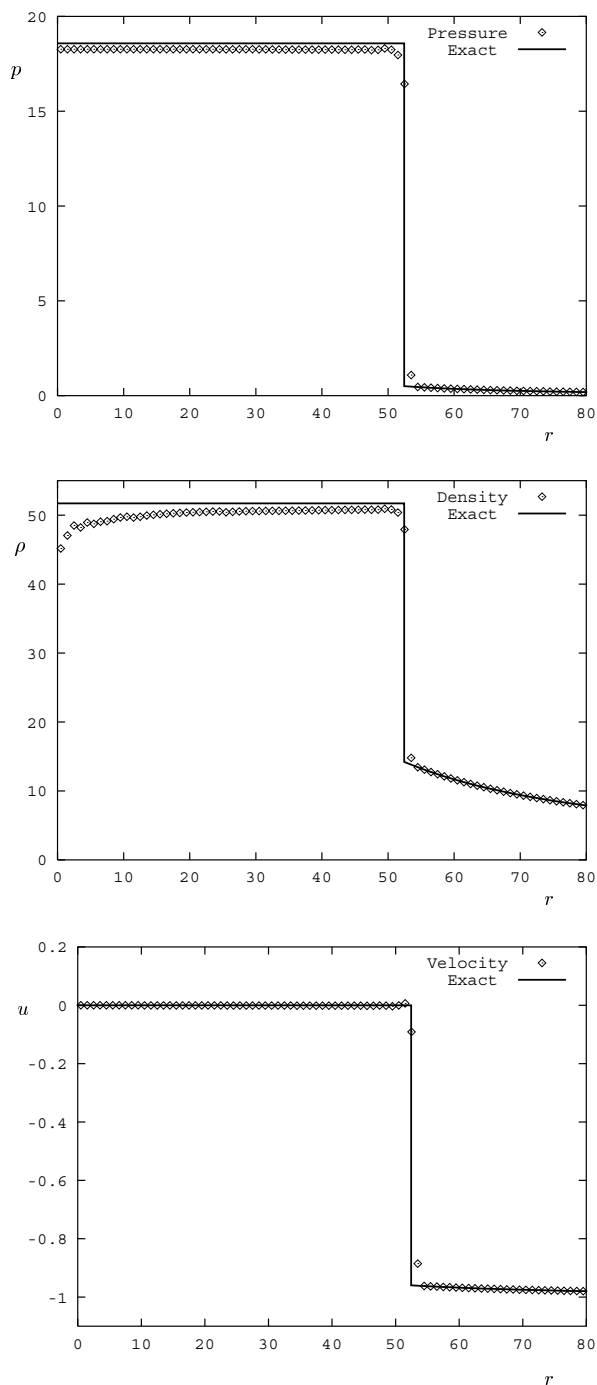
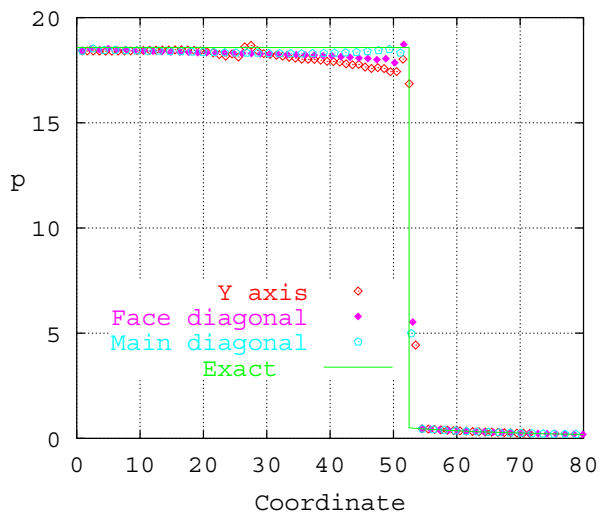**Figure 2.** 1-D computation of spherically converging flow

viates substantially from the "scale-less" self-similar solution.

4.2. Three-dimensional computation

Here we employ the sequence (6) of one-dimensional GRP operators, for the 3-D simulation of the converging flow field. The computation domain is the cube $[0 < x < 70, \ 0 < y < 70, \ 0 < z < 70]$ containing 1/8 of the full sphere, which is divided into a grid of $70 \times 70 \times 70$ cubic cells. The initial conditions are as previously stated, with the velocity vector directed towards the origin. As in the 1-D computation, the CFL-compatible time step is $\Delta t = 0.25$. The boundary conditions on the symmetry planes $x = 0$, $y = 0$, and $z = 0$, are $u = 0$, $v = 0$, $w = 0$, respectively, while on the outer planes $x = 70$, $y = 70$, and $z = 70$, the exact (self-similar) solution for p, ρ, u, v, w is prescribed. The computation was performed to $t = 144$, where the shock front is at about $r_s = 52.5$.

As a first stage of data analysis, we consider the 1-D distribution of flow variables along the following three special lines. A coordinate axis line (e.g., the y-axis); a face diagonal line (e.g., the line $x = y$, $z = 0$); the main diagonal line of the cube $x = y = z$.

Figure 3. Pressure in 3-D spherically converging flow

The results of the operator-split computation, along with the corresponding exact solution, are displayed in Fig. 3 for the pressure, in Fig. 4 for the density, and in Fig. 5 for the radial component of the velocity. Focusing on the post-shock region, most distributions agree fairly well with the exact solution. Deviations are found primarily for the radial velocity along the axis.

In view of this pattern, we have to verify that errors of this magnitude are restricted to narrow strips adjacent to the axes or to the symmetry planes. To this
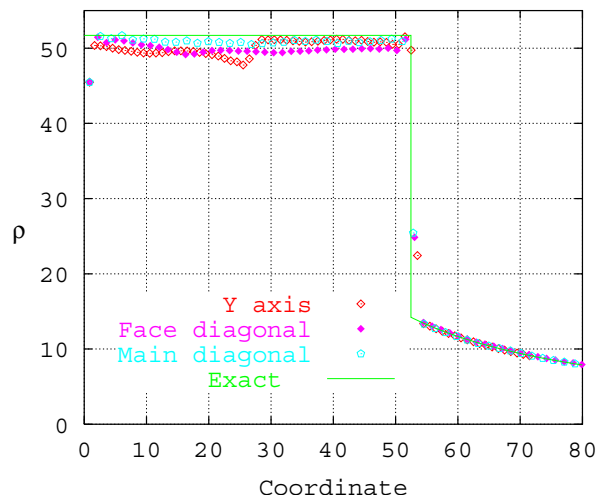
We notice that the simulated shock front is sharp, and agrees well with the exact solution. The pre-shock isentropic flow, as well as the post-shock pressure and velocity agree well with the exact solution, while the post-shock density distribution is somewhat lower than the exact value, in particular near the origin. The obvious interpretation of this result is that near the origin, where the flow is resolved by a small number of cells, the finite-difference approximation de-

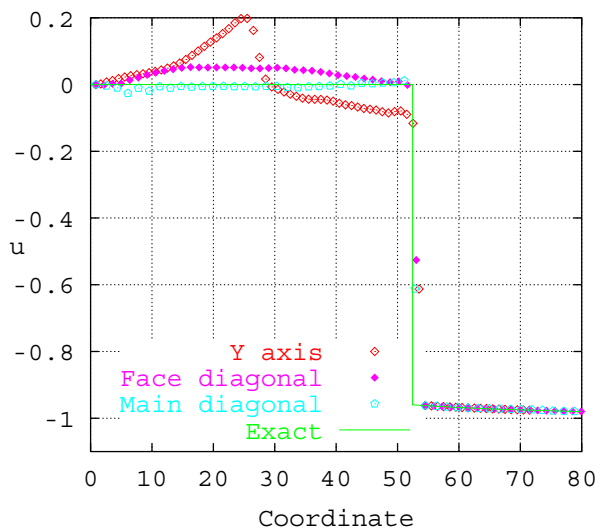**Figure 4.** Density in 3-D spherically converging flow

Figure 5. Radial vel. in 3-D spherically converging flow

end, we inspect in SubSec. 4.4 below the flow field in the cube, using graphical displays of 3-D color maps of the flow. Additionally, since the post-shock flow in the considered test problem is uniform, the difference between the exact values of pressure, density, velocity, and the average of the respective computed variable is a good error indicator. This analysis is presented in SubSec. 4.3 below.

In order to bring out the effects of operator splitting, we also performed a computation of the same flow, using an "unsplit" algorithm (see Sec. 2 above). The corresponding results of the "unsplit" computation exhibit a similar pattern to the split computation, and are summarily presented only in Table 1 below.

4.3. Post-shock averaging

At the conclusion of each computation we evaluated the pressure, density and radial velocity averages for all cells located within the shock front. In the case of 1-D computation, the averaging was weighted by the cell volume. We also evaluated the respective standard deviations, defined as the root-mean-square of the variation of a flow variable about its average value. The results are given in Table 1, where the standard deviations are preceded by a $\pm$ sign.

The mean values of flow variables in the 1-D case deviate from the exact post-shock values by roughly 2% for pressure, 3% for density and 0.07% for radial velocity (the relative velocity error was normalized by the initial value $|u_o| = 1$). It is noted that these error indicators are comparable to the corresponding errors in the mean of the 3-D computation.

The standard deviations of the 3-D solution (both split and unsplit) are larger than the corresponding 1-D deviations by about one order-of-magnitude, which indicates that the 3-D operator splitting produces a "noisier" solution than the 1-D computation. This result is probably related to differences in the shock capturing mechanism of the two schemes.

Table 1. Post-shock averages and deviations.
3-D^{spl} is split computation, 3-D^{uns} is unsplit computation

	p	ρ	u_r
Accur.	18.58	51.70	0
1-D	18.24 ± 0.05	50.65 ± 0.16	-0.0007 ± 0.001
3-D^{spl}	18.13 ± 0.34	50.55 ± 1.57	-0.0027 ± 0.053
3-D^{uns}	18.11 ± 0.37	50.56 ± 1.85	-0.0032 ± 0.059

4.4. 3-D Graphic display

In a 3-D color display each cell is filled out by a color corresponding to the cell-value of the displayed variable. A spectrum bar shows the "color scale" for that variable according to a pre-assigned range. For example, in Fig. 6 we show an oblique view on the density distribution, where the scale increment is $\Delta\rho = 5$. It is noted that since the colored cube is not transparent, the 2-D projection (Fig. 6) shows the distribution only in cells adjacent to the cube faces.

The observed 3-D distribution agrees with the mean density and variation given in Table 1. However, the mean value is a *volume* average, and the view at the *surface* of the cube does not provide information about density variation within the cube. In order to take a look at the interior of the cube, we also display the half-cube obtained by cutting the cube through the diagonal plane $x = y$ (Fig. 7). The variation on the diagonal plane is quite smooth, in support of the contention that there are no "hot spots" in the interior of the cube.

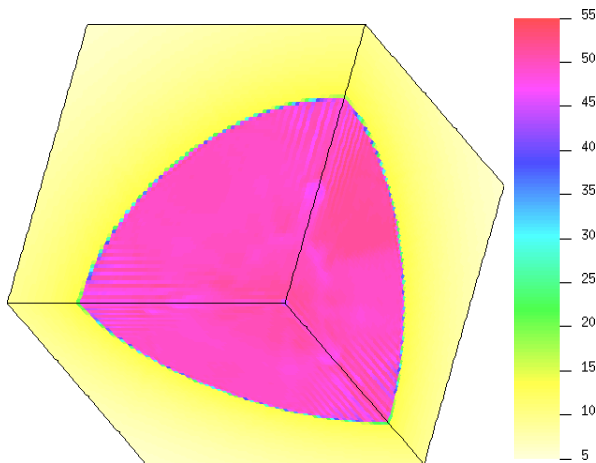According to the 1-D cross-sections in Figs. 3, 4,
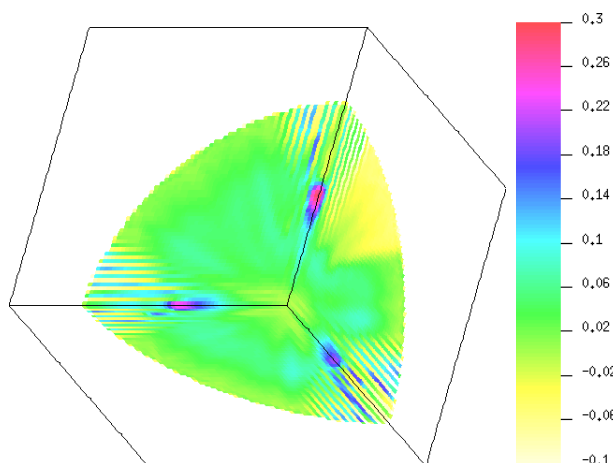
Figure 6. Density in 3-D split computation $t = 144$

Figure 8. Radial velocity in 3-D split computation
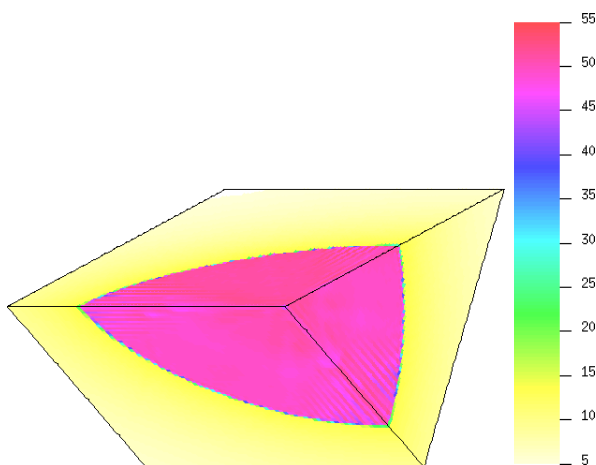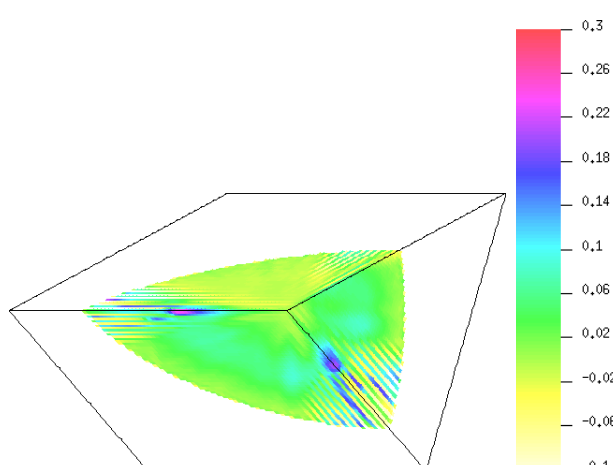

Figure 7. Density in half-cube (see Fig. 6)

Figure 9. Radial velocity in half-cube (see Fig. 8)

5, the largest deviation occurs for the radial velocity along the y-axis. This calls for a color display of the radial velocity in the cube, which is shown in Fig. 8. Here the color scale was chosen to bring out the variation in velocity for the post-shock fluid, discarding the display of the smooth converging flow upstream of the shock wave. It is clear from Fig. 8 that the largest deviations from the exact solution ($u_r = 0$) take place near the axes. Again, the magnitude of these apparent deviations is larger than the respective mean error and variance given in Table 1. Thus, the largest deviation observed on Fig. 8 is 0.2, which is about four times the variance in Table 1.

As before, we take a look at the diagonal half-cube color display of the radial velocity (Fig. 9). It is clear from this display that the variation of radial velocity over the diagonal plane is smaller than along the axes, suggesting that the interior of the cube does not contain "hot spots" comparable to those adjacent to the axes.

5. Conclusions

In this study we have considered the finite-difference approximation to the 3-D hydrodynamic conservation laws obtained by operator splitting, where the GRP scheme was used as the 1-D "solver". The problem adopted for testing the operator-split scheme is a spherically symmetric converging flow, where a stopping shock wave brings the fluid to rest at a uniform state.

Three types of solutions were calculated for this problem. First, an "exact" solution obtained by integrating the set of two ordinary differential equations for the self-similar flow. Second, a 1-D computation of the flow using the quasi conservation laws GRP scheme. Third, a full 3-D computation on a Cartesian grid with cubic cells, performed once with the operator-split scheme, and once with an unsplit integration of the conservation laws. In both the 1-D and the 3-D computations an inflow boundary condition was prescribed at the outer boundary of the domain,

where the flow variables were calculated from the exact (self-similar) solution.

The 1-D computation results exhibit good agreement with the exact solution. In particular, the captured shock front is accurately located and is sharply resolved. The post-shock flow agrees with the exact solution to within a relative mean error comparable to $1/N_s$, where N_s is the number of computational cells traversed by the shock wave (about 2% in the present computations).

The 3-D computation results exhibit a similar pattern "in the mean", in the sense that errors in the post-shock flow relative to the exact values are comparable to the respective 1-D errors. This is taken to imply that "in the mean" the 3-D split scheme produces a captured shock computation comparable to that of the corresponding 1-D scheme. Additionally, as indicated by the 1-D cross-sections of the 3-D computation results, the operator splitting does not degrade the resolution of the captured shock front.

The mean post-shock errors in the 3-D computations tend to be highest along the axes and lowest along the main cube diagonal. We take this to imply that along an axis, where the split integration is dominated by a single 1-D "solver", the 3-D split scheme deviates the most from the respective 1-D symmetric scheme. In other words, considering the 3-D split solution along some radial line, the more symmetric the sequence of 1-D operators is about that line, the better it preserves the geometric symmetry of the flow.

Another revealing indicator in this regard is the standard deviation of the post-shock flow (Table 1). It shows that the level of fluctuations introduced by 3-D shock capturing is about an-order-of-magnitude higher than the respective 1-D fluctuations. We interpret this result as indicating a difference in the shock capturing mechanism of the two schemes – the 3-D split scheme and its 1-D symmetric counterpart.

In summary, this study brings out various aspects of the interplay between the 3-D Cartesian operator splitting and the geometrical symmetry of the considered flow field. Comparing 1-D symmetric and 3-D split shock capturing, the solution associated with the latter is "noisier" than, yet just as accurate "in the mean" as, the symmetric 1-D solution.

References

Ben-Artzi M, Falcovitz J (1984) A Second-Order Godunov-Type Scheme for Compressible Fluid Dynamics. J Comput Phys 55: 1–32

Ben-Artzi M, Falcovitz J (1986) An Upwind Second-Order Scheme for Compressible Duct Flows. SIAM J Sci Statist Comput 7: 744–768

Ben-Artzi M, Birman A (1990) Computation of reactive duct flows in external fields. J Comput Phys 86: 225–255

Falcovitz J, Ben-Artzi M (1995) Recent Developments of the GRP Method. JSME Intl J. B 38:497–517

Strang G (1968) On the construction and comparison of difference schemes. SIAM J Num Anal 5:506–517

Noh W F (1987) Errors for calculations of strong shocks using artificial viscosity and an artificial heat flux. J Comput Phys 72: 78–120

Taylor G I (1946) The air wave surrounding an expanding sphere. Proc Roy Soc. A 186:273–292. Also in "The scientific papers of G. I. Taylor", pp. 412–478. G. K. Batchelor, Editor. Cambridge University Press, London, 1963.